## INSTRUMENTATION AT THE IBR-2

### DN-6 diffractometer

The straight end section of a 7-m mirror neutron guide was replaced with a focusing device with vertical parabolic geometry for studies of microsamples under extreme conditions (**Fig. II-1-1**).

***Fig. II-1-1.*** *Neutron focusing device with vertical parabolic focusing at the DN-6 diffractometer.*

The gain factor in the intensity of the incident neutron beam was estimated to be about four.

### FSD diffractometer

On the FSD diffractometer, heating control during experiments with metal samples by electric current up to 800°C (with temperature control) on a mechanical uniaxial testing machine LM-29 became possible. It allows one to study the behavior of structural materials under external uniaxial stresses of both tensile and compressive types, up to a maximum value of 29 kN directly in a neutron beam. This opens up new opportunities for studying thermomechanical characteristics of materials *in situ* when combining external stresses and high temperatures. Special software ReMeSys makes it possible to specify any necessary combination of values of external stress and temperature on the sample under study.

In the framework of tests of the testing machine at FSD, several neutron diffraction experiments were successfully performed with stretching/compressing of samples from constructional materials (steel, alloys) at various temperatures. Thus, for a widespread aluminum alloy D16, the degradation of elastic characteristics of the material subjected to uniaxial tension was studied for different values of the sample temperature (**Fig. II-1-2**, a). The accuracy of determination of crystal lattice deformations at the FSD diffractometer proved to be rather high, which made it possible to reliably observe the difference in ε(σ) curves for different temperatures and estimate the changes in the elastic properties of the material as a function of temperature. Using the results of the experiments, it was found that the modulus of elasticity of the material monotonically decreases from 76 to 62 GPa in the temperature range of 13-150°C (**Fig. II-1-2**, b). The analogous temperature dependence was also observed for the ultimate strength of the material.

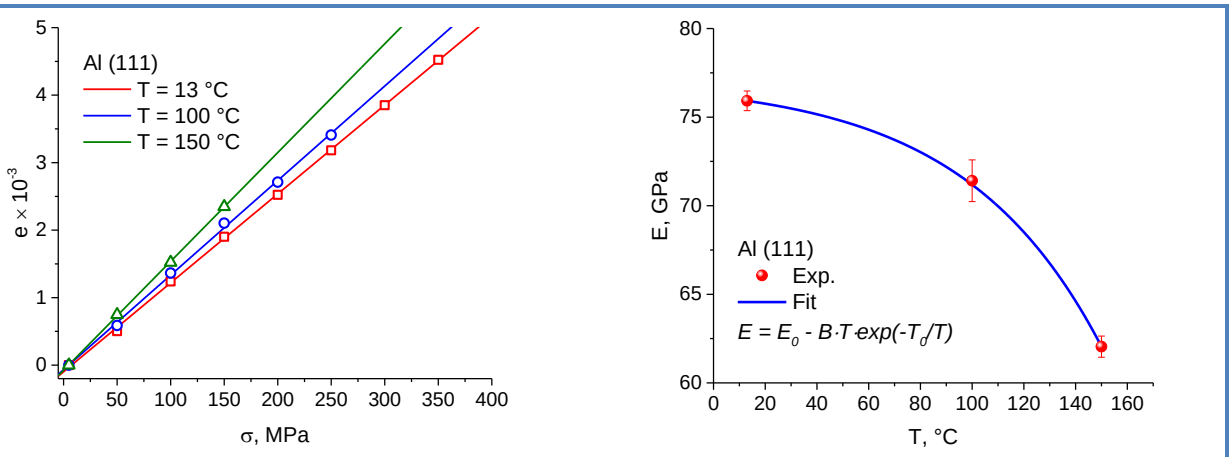


*a)* *b)*

***Fig. II-1-2.*** *a) Crystal lattice deformation for peak (111) in aluminum alloy D16 versus the applied stress measured at different temperatures. b) Temperature change in the elastic modulus of alloy D16.*

In addition, on FSD, the work was continued on improving the algorithms for reconstructing diffraction spectra from "raw" data registered in the list-mode. In particular, the version of the algorithm for multi-detector systems was implemented, which allows one to simultaneously reconstruct high-resolution spectra from all connected detectors or detector elements with individual parameters of the time-of-flight scale. This made it possible to realize separate spectrum accumulation and precise electronic focusing for individual elements of the back-scattering detector BS, which resulted in a better line shape and higher detector resolution.

**FSS diffractometer**

On beamline 13 of the IBR-2 reactor, in cooperation with the SC department, the work on the construction of the FSS Fourier diffractometer is in progress. In 2017, a Fourier-chopper was installed in the mirror neutron guide and put into opertation (**Fig. II-1-3, a**). The diffractometer control software on the basis of SONIX+ was installed. The optimum positions of individual photomultipliers of the second 90°-detector West for the new geometry were calculated, followed by the detector assembling and connection. In front of both 90° Ost and West detectors, radial collimators were installed (**Fig. II-1-3, b**).

First test experiments were performed in a high-resolution mode (RTOF-mode) with the Ost and West detectors to estimate the quality of geometric alignment of individual photomultipliers, as well as to estimate the resolution function of the diffractometer (**Fig. II-1-4**). Data from both 90°-detectors are accumulated by a new MPD-32 analyzer in the list-mode, which allows one to flexibly set parameters of the time-of-flight scale, introduce necessary corrections and ensure high accuracy of electronic focusing for individual detector elements.

a) b)

***Fig. II-1-3.*** *a) Fourier-chopper of FSS installed in-between the sections of the mirror neutron guide. b) Sample position at FSS. The photo shows the end of the mirror neutron guide, goniometer with a sample, Ost and West detectors with radial collimators installed in front of them.*

To improve the diffractometer characteristics, it is planned to replace the mirror neutron guide together with the vacuum housing. For this purpose, calculations were performed and basic parameters of a new neutron guide were determined, which will allow a several-fold increase in the flux density in the short wavelength range. The neutron guide is designed as parallel-sided in the horizontal plane (window width 10 mm) and linearly converging in the vertical plane (heights of entrance and exit windows are 126 and 50 mm, respectively).

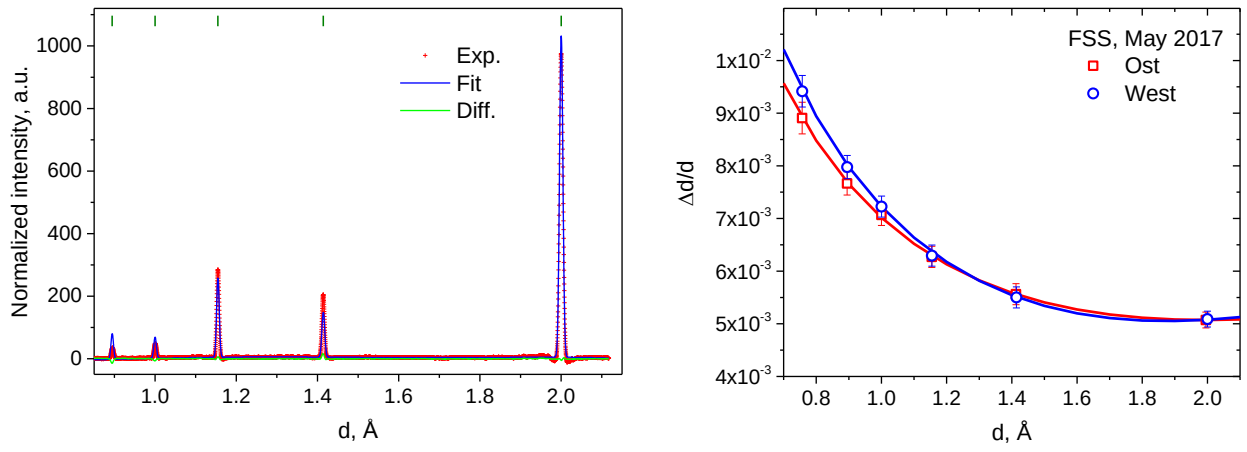


a) b)

***Fig. II-1-4.*** *a) First high-resolution spectrum from ARMCO iron sample measured by the Ost detector of FSS with the refinement using the Rietveld method. b) FSS resolution function measured at the maximum chopper speed Vmax = 2000 rpm.*

A super-mirror Ni/Ti-based glass coating with the critical index m = 2 is projected. At present, the manufacturing and installation of mirror sections and vacuum housing of the neutron guide are in progress. In addition, it is planned to install a new automated aperture at the exit of the mirror neutron guide, which will make it possible to regulate dimensions of the incident neutron beam at the sample under study. A contract was concluded with the company JJ X-RAY (Denmark); the manufacturing of the device is in progress.

**EPSILON diffractometer**

The EPSILON diffractometer was equipped with a three-axis high-pressure cell to produce deformations in porous rock samples (length 60 mm, diameter 30 mm) in a neutron beam by applying axial stress, confining pressure and pore pressure. The axial pressure can vary in the range of up to 150 MPa, confining pressure – up to 70 MPa and pore pressure – up to 70 MPa. All three load types change independently, so the deformation rate can be controlled individually.

**GRAINS reflectometer**

On the GRAINS multifunctional reflectometer, controllable beam collimating apertures to improve the background conditions at the sample position were designed, manufactured and successfully tested (**Fig. II-1-5**).

The control function over the slit-type apertures was added to the SONIX software of the control computer, which makes it possible to remotely specify the required neutron beam dimensions directly at the sample position.

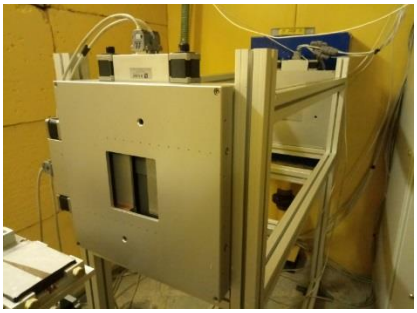

***Fig. II-1-5**. Controllable slit-type apertures for collimating beam directly at the sample position on the GRAINS reflectometer.*

**REMUR reflectometer**

On the REMUR reflectometer, a polarization analyzer with a cross section of 20×20 cm$^2$, consisting of 150 supermirrors (**Fig. II-1-6**), was put into operation.

*a)*

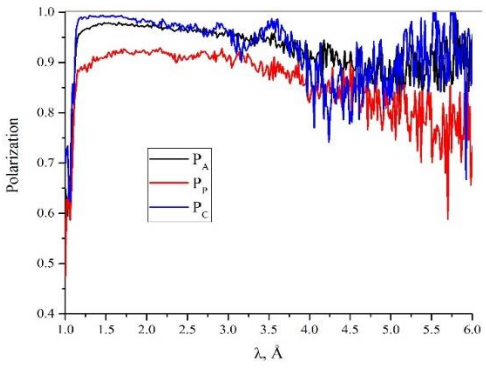


*b)*

***Fig. II-1-6.** (a) Polarization analyzer with a cross section of 20×20 cm2 at the REMUR reflectometer. (b) Long-wavelength dependences of the neutron polarization efficiency of polarizer Pp (beam cross section 40 × 2.5 mm) and neutron polarization analyzer Pa (grazing angle 3.5 mrad).*

Investigations of neutron channeling in planar waveguides were continued [1]. Planar neutron waveguides convert a conventional neutron beam with a width of 0.1 to 10 mm into a very narrow divergent beam with an initial width of about 0.1 μm, which is then used to scan local microstructures in the volume with a high spatial resolution. An important characteristic of planar waveguides is the channeling length (distance at which the neutron wave attenuates within the

waveguide by a factor of *e*). To determine expermentally the neutron channeling length as a function of the waveguide parameters, a neutron absorber was placed on the surface of the film, and the microbeam intensity from the end of the waveguide was measured by varying the absorber length. It was found that the neutron channeling length grows exponentially with increasing thickness of the upper layer, decreases for higher resonance orders (n = 0, 1, 2) following the function ~1/(n + 1) and shows a linear increase with increasing depth of the potential well of the waveguide (**Fig. II-1-7**). The experimental results confirm the qualitative theoretical predictions.

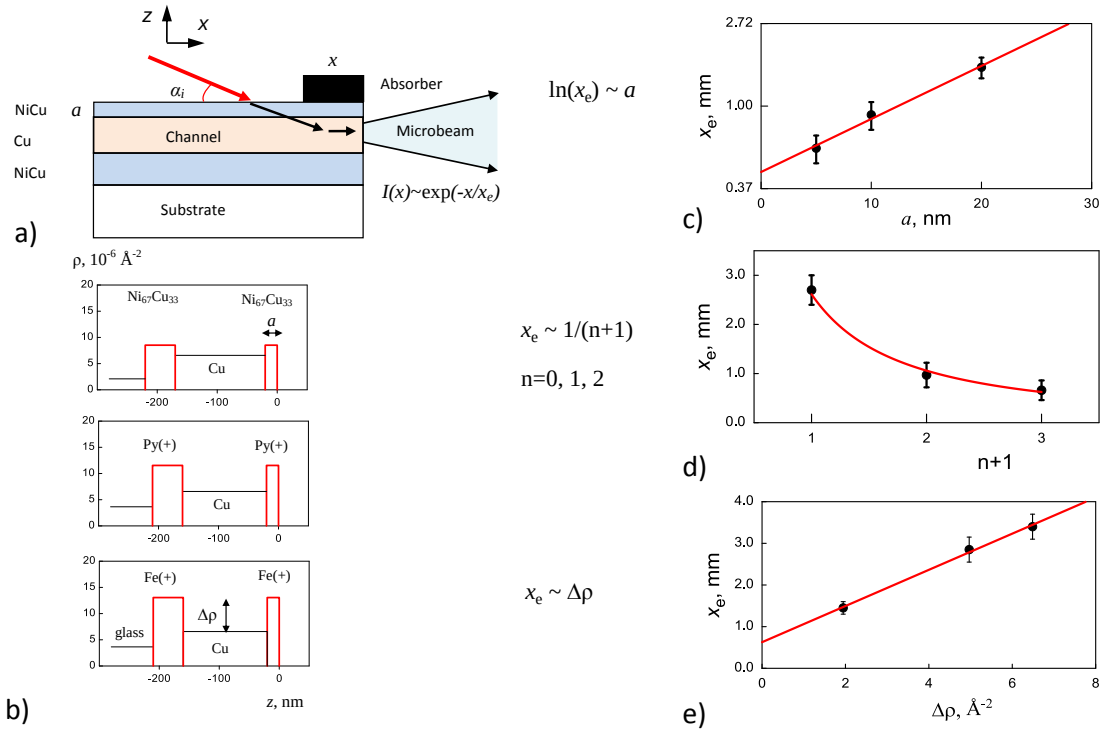


***Fig. II-1-7.*** *(a) Design of the experiment (a). Potential of interaction of neutrons with the structure (b). Dependences of channeling length on thickness of the first layer (c), order of resonance mode (d) and depth of the potential well (e).*

**REFLEX reflectometer**

The reconstruction of the REFLEX reflectometer on beamline 9 of the IBR-2 reactor into a spin-echo small-angle neutron scattering (SESANS) spectrometer was continued. The main task was to test the performance of spin rotators produced by the Research Center of Jülich (Germany). Spin rotators *A, B, C, D* were installed at the sample position of the REFLEX reflectometer in a permalloy shielded chamber in accordance with the design of the SESANS spectrometer, as shown in **Fig. II-1-8**. Each of the spin rotators was individually supplied with a constant current of 10 A, which induced periodic oscillations of the polarization vector of the beam passing through the spin rotators. The magnetic field in the spin rotators is directed along their axis in parallel to the larger side; the beam polarization is perpendicular to the magnetic field of the spin rotators and is directed along the Z-axis. Test measurements of the so-called spin-echo focusing without a sample—an important characteristic of any spin-echo spectrometer—were carried out. When the lengths of two arms are equal and the modulus of magnetic fields are the same at the same time, the z-component of polarization, $P_z$, should not change as neutrons pass consecutively the two arms. In case when pulsed magnetic fields are used, this statement is valid not for the entire

wavelength range, but only for certain intervals [2]. When generating time-linear field pulses with a frequency of 400 Hz and an amplitude of about 100 Gs, a quasi-plateau was obtained in the $P_z(\lambda)$ dependence. The spin-echo focusing curves were measured in the spectral ranges corresponding to the quasi-plateau. One of the arms was varied within the spatial limits available inside the chamber. The obtained curves are shown in **Fig. II-1-8**. Insufficient damping of oscillations is explained by a small amplitude of the linear field pulse, as well as by a low pulse repetition rate. Nevertheless, the curves are satisfactorily described by the model function, which confirms the observation of spin-echo focusing. On the basis of the results of experimental tests, the electronic power scheme was redesigned and the spin rotators themselves were upgraded, which would significantly reduce the power of electronics and simplify the control of the spin rotator current.

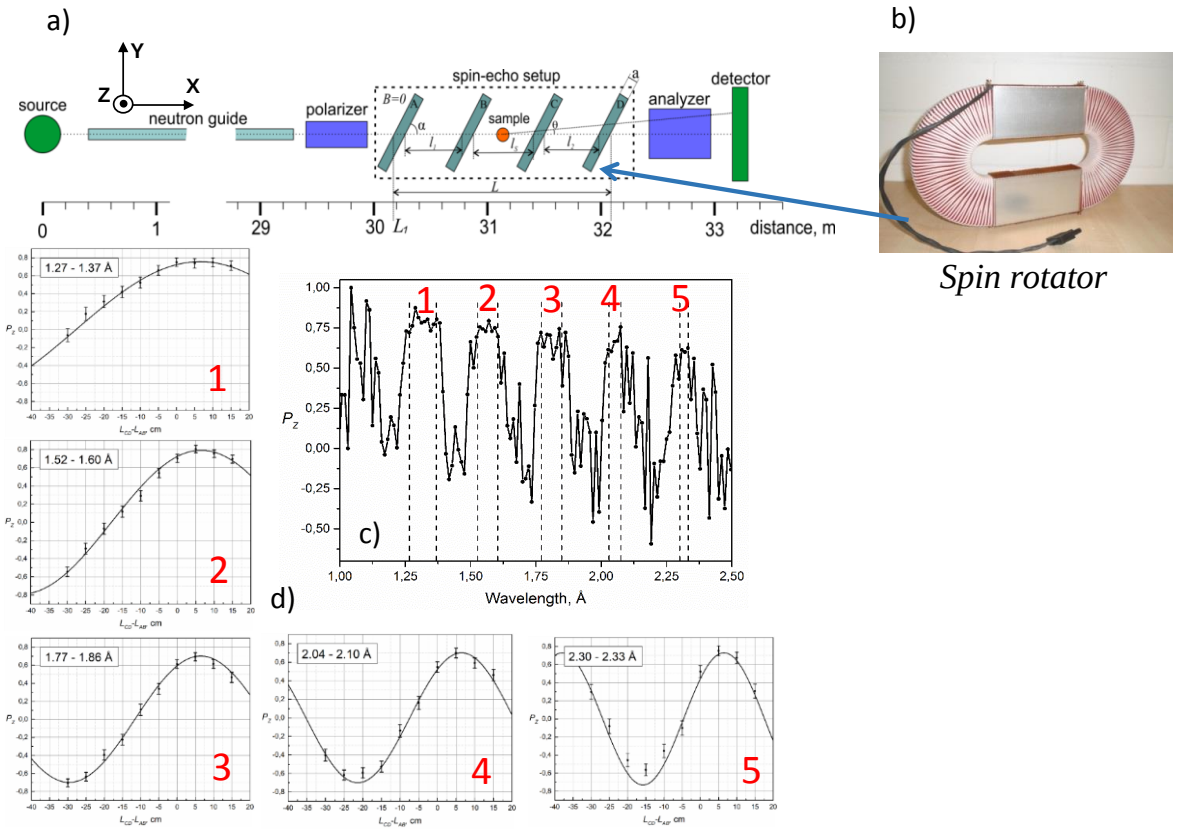


*Fig. II-1-8. Scheme of the spin-echo small-angle neutron scattering spectrometer (a). Spin rotator used in the experiment consists of four separate electromagnetic coils forming a closed magnetic circuit (b). Wavelength dependence of polarization of the neutron beam that passed two spin-echo arms (c). Spin-echo signals for different wavelength ranges (1,2,3,4,5). The solid line denotes theoretical calculations (d).*

**YuMO spectrometer**

The upgrade of the YuMO spectrometer was continued. The main areas of activities included the design of a new replaceable collimator, development of sample environment and studies related to the application of the chopper. In addition, work is underway with a position-sensitive detector of a new type, which is to be put into operation. The spectrometer software was upgraded

and extended. In particular, in cooperation with the SC department algorithms were developed and tested in the measurements using a new spectrometer positioning program. In cooperation with LIT, algorithms for the SAS program were developed and tested. It was shown that the overlapping method realized in these algorithms not only provides a qualitatively new level of small-angle neutron scattering curves, but also allows one to improve statistics in the range of the overlapping curves from different detectors [3]. The experiments with the delay of the chopper made it possible to optimize this parameter. In addition, possibilities for improving the obtained spectra from weakly scattered samples by doubling the rotation frequency of the chopper were considered. A technical design for the collimator in general and its units in particular was proposed. The necessary calculations were made to simulate the scattering at the spectrometer with a model collimator.

Experiments were carried out to estimate the necessary time per measurement at the YuMO spectrometer. Two variants with one and two detectors were considered. It was shown that the two-detector experimental scheme reduces the required exposition time by more than half. In solving structural problems using modern software, the two-detector system provides a new qualitative level of data for further analysis. The results of the work can be used in planning experiments at the YuMO spectrometer and during the modernization of the instrument, as well as at other time-of-flight spectrometers.

### NRT spectrometer

For the neutron radiography and tomography spectrometer, a modernized two-mirror CCD-based detector system was manufactured. Its application will improve the spatial resolution of experimental data.

### References

[1] Kozhevnikov S.V., V.D. Zhaketov, Yu.N. Khaydukov, F. Ott, F. Radu, Channeling of Neutrons in a Planar Waveguide, JETP 125 (2017) 1015-1025.

[2] Bodnarchuk V., V. Sadilov, S. Manoshin, R.V. Erhan, A. Ioffe, Journal of Physics: Conf. Series 862 (2017) 012003.

[3] Soloviev A.G., T M Solovjeva, O I Ivankov, D V Soloviov, AV Rogachev and A I Kuklin. SAS program for two-detector system: seamless curve from both detectors. IOP Conf. Series: Journal of Physics: Conf. Series 848, 1, (2017) 012020.

## NOVEL DEVELOPMENT AND CONSTRUCTION OF EQUIPMENT FOR THE SPECTROMETER COMPLEX

### Complex of cryogenic neutron moderators

In 2017, the pelletized cold moderator CM-202 successfully operated for physical experiments in the 2nd, 4th and 8th cycles of the IBR-2 reactor operation at a power of 2 MW. In the 8th cycle, the cold moderator CM-202 operated with a new cryogenic system, which made it possible to reduce the temperature in the moderator chamber by 8 K (down to 23 K) at a reactor power of 2 MW as compared to the previous cryogenic system. This allowed a significant increase in the yield of cold neutrons from the surface of the cold moderator. In addition, the new cryogenic system was tested under simultaneous cooling of the CM-202 cold moderator chamber and CM-201 test stand at a zero reactor power. The results showed that the use of the new cryogenic system allowed a three-fold reduction in temperature (down to 20 K) in both chambers as compared to the previous cryogenic system.

To investigate the possibility of extending the cold moderator operation time for physical experiments, work is under way to study the amount of hydrogen produced in the moderator material (mixture of mesitylene and m-xylene) after irradiation during one reactor cycle (~ 11 days). For this purpose, a setup with a closed cycle cryorefrigerator was designed and assembled, in which a chamber with a sorbent was cooled to absorb hydrogen present in helium after mesitylene decomposition in a neutron beam. As a result of the experiment it was preliminarily found that the content of the by-product gas fraction of hydrogen in helium at the end of the reactor cycle with cold neutrons may amount to 5% or more in molar terms. These results require further validation by alternative methods.

On the basis of the developed technical specifications, the following elements of the control system of the CM-201 cold moderator were installed and successfully tested: thermometric sensors, control system of cryogenic valves for the new cryogenic system, new software (**Fig. II-2-1**).

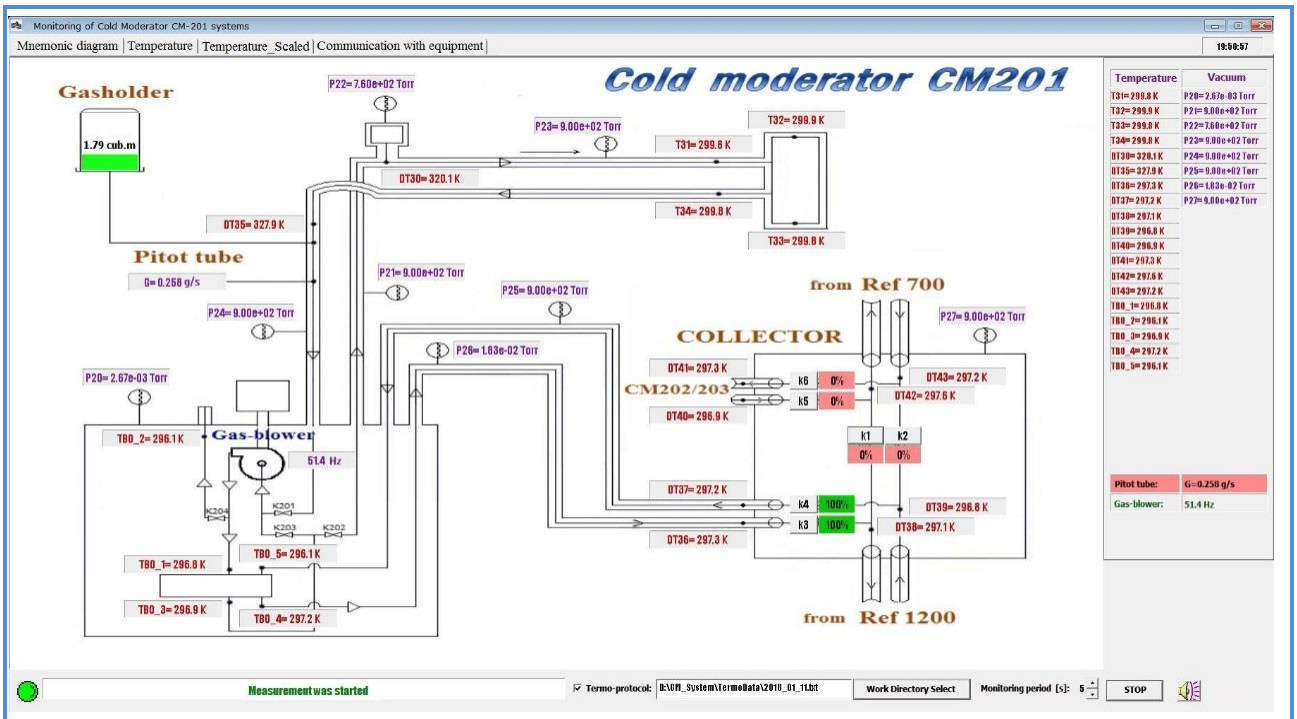


*Fig. II-2-1. Control program for the CM-201 pelletized cold moderator with a new cryogenic system.*

Technical specifications for a screw-type discharging device for the CM-201 moderator were developed. This device is designed for continuous replacement of the moderating substance in the moderator chamber.

**Radiation research facility**

In 2017, the following activities were performed on the radiation research facility at IBR-2:

- new control panel for facility transfer was successfully tested and put into trial operation;
- biological shielding was installed, thus significantly improving radiation conditions on IBR-2 beamline 3;
- technical specifications were developed for installation of a robotic arm for handling highly active samples;

- in cooperation with the Laboratory of Magnetic Sensors of the Lviv Polytechnic National University, the investigation of radiation resistance of magnetic sensors (3D Hall sensors) was continued within the framework of international projects for the development of ITER and DEMO
- fusion reactors;
- in cooperation with DLNP, VBLHEP JINR and BSTU (Republic of Belarus) experiments on the irradiation of samples of silicon scintillators were conducted to study changes in their electrical and physical properties under irradiation;
- In cooperation with VBLHEP JINR, Academy of Sciences of the Republic of Uzbekistan and Ural Federal University (Yekaterinburg) we continued the investigation of the nature of radiation-induced defects in topaz samples (radiation staining) (**Fig. II-2-2**), as well as exploration of possibilities of producing medical isotopes at IBR-2 beamline 3.

***Fig. II-2-2.*** *Topazes after irradiation at IBR-2 beamline 3.*

**Future pulsed neutron source at JINR**

In 2015-2017, with an active participation of specialists from the FLNP Spectrometers' Complex Department, possible variants of the future pulsed neutron source at JINR were considered and analyzed, since the service life of the IBR-2 reactor is expected to expire by about 2032. In 2017, we convincingly demonstrated that a fissionable isotope of neptunium ($^{237}$Np) is more preferable to be used as a nuclear fuel for a high-intensity pulsed neutron source (both in a variant of a pulsed periodic reactor and in a variant of a multiplying neutron-producing target of a proton accelerator) than plutonium-239. The advantage lies not only in the abandonment of the use of a weapons-grade nuclear material, but also in the possibility of obtaining much shorter bursts of thermal neutrons (20 μs instead of 200 μs) with a record peak flux density up to $10^{17}$ n·cm$^{-2}$·s$^{-1}$, which is an order of magnitude higher than the same value for the most intense European source ESS with a proton beam power of 5 MW (to be put into operation in 2019). In addition, the background noise power in a neptunium-based source will be 2-2.5 times less than in the reactor based on other fissile materials, and the duration of reactor operation without refueling will be significantly increased (15-20 years). The work done can serve as a basis for the development of a detailed design of the future source (**Fig. II-2-3**).

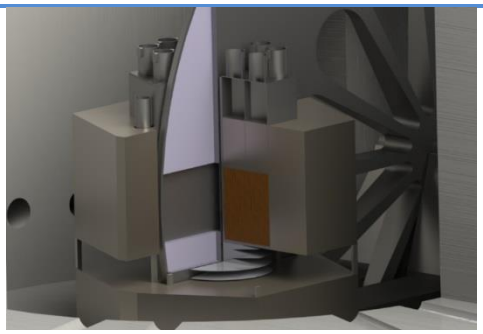

***Fig. II-2-3.*** *Model of $^{237}$Np-based reactor.*

**Calculations and simulation of spectrometers**

In 2017, we continued the development and support of the modules of the program for simulating neutron spectrometers and experiments for VITESS (Virtual Instrument Tool for European Spallation Source). Almost half of all VITESS modules have been developed in FLNP; in particular, the tasks of simulating neutron instruments for polarized neutrons have been almost completely carried out. The simulation of spin-echo spectrometers with time-dependent magnetic fields and model systems has been successfully performed. The magnetic fields can be both

model (built into modules) and calculated by an external program (MagNet, Ansys, etc.). Virtually all existing neutron-optical elements (neutron guides, benders, mirrors, lenses, prisms and their combinations) have been built into VITESS (and successfully used) as well as the possibility of simulating neutron detectors (including position-sensitive ones) with time focusing has been provided. More detailed information about VITESS can be found in the review article of the jubilee issue of the journal "Physics of Elementary Particles and Atomic Nuclei" (Volume 47, Issue 4, pp. 1228-1248) devoted to the 60th anniversary of JINR.

In 2017, the development of special mathematical models and corresponding programs for simulating full reflectometric and GISANS experiments with samples, including multilayer rough samples and magnetic scattering, was completed. Various modifications of the kinematic approximation were developed and analyzed taking into account the penetration depth, refraction, final resolution of the instrument, and renormalization of collected data.

It has been shown that the modified kinematic approximation used in the simulation of specular reflection, which takes account of the effect of neutron wave refraction at an interface, gives fairly good agreement with the available experimental data and the Parratt method, which is considered to be the most accurate method of the dynamic theory.

Two systems with a silicon matrix were considered. In the near-surface layer of the systems, cubic nickel nanoparticles (edge length 150 Å) were distributed to form a 3D tetragonal lattice. For the primitive tetragonal Bravais lattice the parameters were $a = b = 400$ Å, $c = 500$ Å, while for the body-centered lattice – $a = b = 400$ Å, $c = 1000$ Å. A layer of silicon 50 Å thick was placed above the first layer of nanoparticles, and only four layers of nanoparticles were distributed in the depth of the sample. Ten periods in each direction were chosen in the lateral plane. For this problem, the penetration depth of the neutron wave was not introduced and the resolution of the spectrometer was not taken into account.

The results of simulations of full diffraction patterns for the two systems described above using the modified kinematic approximation are presented in **Fig. II-2-4**.

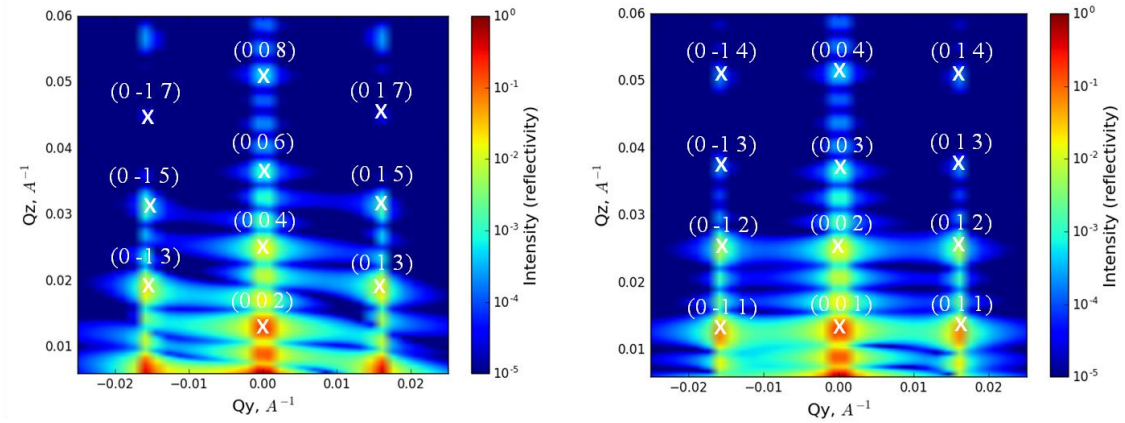


***Fig. II-2-4.*** *Results of simulations of full diffraction patterns using the modified kinematic approximation for a system with a silicon matrix, in the near-surface layer of which cubic nickel nanoparticles (edge length 150 Å) are distributed. Simulations for body-centered (left) and primitive (right) tetragonal Bravais lattices are presented. Miller indices of observed diffraction peaks are given. Crosses indicate theoretically calculated positions of diffraction peaks. In the diffraction pattern, oscillations from the total thickness of the modeled sample are clearly observed. Calculation time for each pattern was about 1 h (using processor Intel Core i5, 2.5 GHz).*

At the left, systematic extinctions characteristic for the body-centered tetragonal lattice are clearly visible. At the same time, at the right, there are no systematic extinctions in the diffraction

pattern, as it should be in the case of a primitive lattice. In both cases, the lateral lattice parameters ($a = b = 2\pi\ 0.0157 = 400$ Å) can be found from the obtained diffraction spectra.

It should be noted that the diffraction pattern in the specular channel of neutron reflection is identical in both cases of the tetragonal distribution of nanoparticles in the matrix. Consequently, from specular reflection data one can evaluate only the distance between the nearest nanoparticle layers and the total number of layers in the sample, while the type of spatial ordering of nanoparticles in the matrix cannot be determined.

The problem of simulating specular reflection from a system of cubic nickel nanoparticles (edge length 400 Å) forming a square lattice (lattice parameter 1200 Å) on the surface of a nickel substrate was solved as well. It was assumed that the cubes were placed in an organic solvent with a scattering length density corresponding to that of ribonucleic acid (RNA) which is approximately half the value characteristic for natural nickel.

The results of 3D simulation of a full reflectometry experiment are given in **Fig. II-2-5**. At the left, the results are shown for the case when the dimensions of all cubic nanoparticles were identical, at the right – when the height of all cubic nanoparticles was the same but the sizes of the lateral cross-section were varied randomly in the range from 100 to 400 Å. It is interesting to note that for an ideal system of cubes, the extinction of the third-order reflection 03*l* for $Q_Y = \pm 0.0156$ Å$^{-1}$ is clearly observed (**Fig. II-2-5**, left).

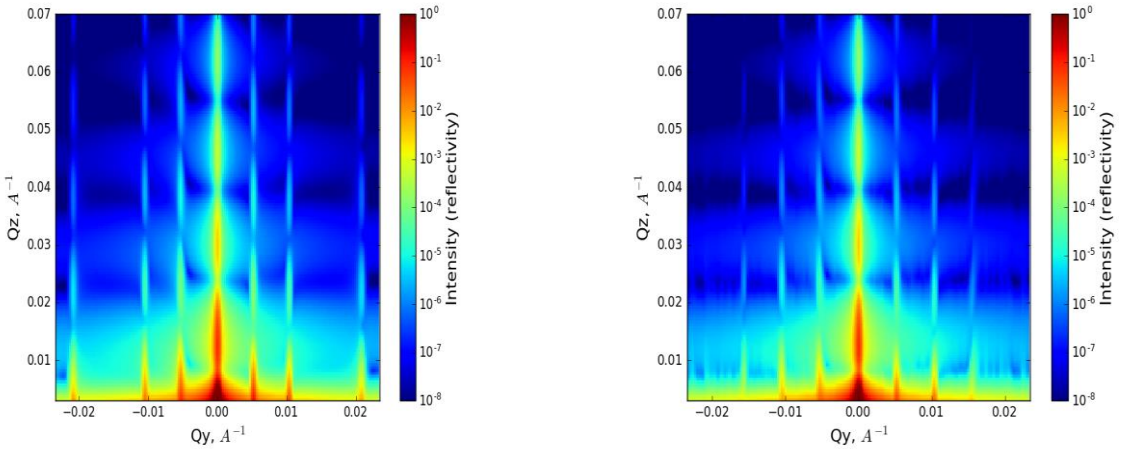


***Fig. II-2-5.*** *Simulation of a full reflectometry experiment for a system of cubic nickel nanoparticles in an organic solvent on a nickel substrate (spectrometer resolution is not taken into account).*

These extinctions can be explained by the multiplicity of lateral sizes of nanoparticles and the period of the square lattice formed by these nanoparticles. The introduction of a random distribution over lateral nanoparticle sizes results in the reappearance of this reflection, but higher-order diffraction reflections (in this example, already the fourth-order reflections) are greatly suppressed in intensity and would be practically invisible in a real experiment.

### Cryogenics and vacuum systems

Major activities in this area were carried out in accordance with the project “Development of PTH sample environment system for the DN-12 diffractometer at the IBR-2 facility” aimed at developing a cryostat for temperature and magnetic investigations of condensed matter under pressures of up to 10 GPa at the DN-12 spectrometer. A significant extension of the range of scientific problems solved by means of this diffractometer has required the construction of a cryostat with a variable temperature (in the range of 300 - 4 K) and magnetic field (0 - 4 T), which will allow us to distinguish between the effects from various types of interactions when studying

complex magnetic structures, build detailed magnetic phase diagrams of magnets under study and thoroughly investigate mechanisms of magnetic phase transitions.

The magnet is a Helmholtz pair of magnets made of a high-temperature superconducting tape of the second generation YBCuO (manufactured by "SuperOx", Russia). The magnet is cooled by a closed-cycle cryocooler. The cryostat with a high-pressure cell, which in its turn is cooled by another closed-cycle cryocooler, is inserted into the center of the magnet through a horizontal shaft. The temperature of the cell is regulated by a controller in the range of (4 - 300) K.

The project is being implemented in cooperation with the National Institute of Research and Development in Electrical Engineering (ICPE-CA) Bucharest, Romania.

The following major activities have been carried out in the framework of the project:

- Design documentation for the cryostat and magnet producing a magnetic field of 4 T was prepared.
- Machine for HTS tape winding was developed and manufactured;
- Cryostat for cooling the magnet was manufactured.
- Magnet and coils were produced.
- Horizontal cryostat for cooling high-pressure cells was manufactured and tested. This cryostat with a high-pressure cell is inserted into a magnetic field of the superconducting magnet.
- Power source for the superconducting magnet with an operating current of up to 300 A was put into operation.
- Preliminary tests of the cryostat with a magnet were carried out at a current of 90 A. The magnet constant was measured to be 0.0154 T/A. A magnetic field of 1.386 T was obtained. Photos of this equipment and temperature graphs of different parts of the cryostat are shown in the FLNP Annual Report for 2016. The achieved terminal temperatures of the magnet prototype (16 K), warm ends of HTS current leads (58 K), and sample (2.8 K) correspond to the design values.

In April 2017, when carrying out the start-up and adjustment work together with the Romanian colleagues, we repeated test experiments and detected the degradation of the properties of the tape in one of the magnet coils, which showed up as a decrease in the critical current value and, correspondingly, the magnetic field strength. Further studies revealed the degradation of the properties of the tape in the second coil as well.

To determine the causes of the observed effect, we carried out additional studies, which showed that the most probable reason is the discrepancy between the actual characteristics of the tape and the characteristics specified by the supplier.

When current was introduced into the magnet, it was found that at a current of 105 A, an avalanche-like increase in the potential of the coils (quenching) occurs. To identify the reasons for the growth of the potential, the magnet was dismantled, and each coil was tested separately. The coils consist of three continuous pieces of the tape connected by soldering. The resistance of each solder junction does not exceed 20 nΩ at 77 K. The resistance of the junctions becomes lower with decreasing temperature. At a current of 60 A, the potential of the coil was 4.3 mV at a temperature of 16 K and 10.8 mV at 35 K; the corresponding resistances were 70 and 180 μΩ. As can be seen, the coil resistance is three orders of magnitude greater than the resistance of the junctions, which is indicative of the absence of superconductivity along the entire length of the tape.

The quality control of HTS tapes is performed by the manufacturer by running the tape through liquid nitrogen and measuring the potential of a piece of tape about 1 m long. At this length, the potential value is close to the noise level in the measuring device (we also tested a piece of tape 75 cm long and there was no resistive component in it).

For the tape in the coil (length 750 m), the potential was found to be non-zero and was clearly detected by a microvoltmeter. The existence of the potential across the coil results in a heat release (0.75 W at a current of 75 A), so the coil quickly overheats and quenches.

Visual inspection revealed the peeling-off of the copper coating from the HTS tape (**Fig. II-2-6)**. On the basis of the obtained results, it can be concluded that the HTS tape from "SuperOx" is unsuitable for manufacturing superconducting magnets.

***Fig. II-2-6.*** *Peeling-off of the copper coating from the HTS tape.*

The negotiations with the supplier in order to find out the reasons for the tape degradation and eliminate the problems have yielded no results, therefore it was decided to change the supplier of the superconducting tape and extend the project period. SuperPower Inc. (USA) was selected as a new supplier of the HTS tape, while accessories and magnet will be manufactured by the ICPE-CA Institute (Romania). At present, corresponding contracts have been concluded with these organizations. The coils made from SuperOx tape can be used in a liquid-nitrogen-cooled cryostat (temperature of about 65 K with pumping) to generate fields in the range of 0.4 to 0.8 T depending on whether one or two coils are used.

It should also be noted that to install the magnet on the DN-12 diffractometer, it is necessary to upgrade the housing of the diffractometer, as well as to conduct an inspection of the existing equipment to ensure its effective operation in magnetic fields.

In 2017, the spectrometer DIN-2PI was equipped with a cryostat with a closed-cycle pulse tube cryorefrigerator. A series of tests of the cryostat were carried out to optimize its thermal performance.

At the NERA spectrometer, the defective cryorefrigerator CRYOMECH PT405 was replaced with a cryorefrigerator SUMITOMO SRDK-415 with a change in the design of the thermal bridge between the sample shaft and the second stage of the cold head of the cryorefrigerator, making it possible to lower the minimum temperature at the sample position from 6 K to 5 K.

Work has been completed on the commissioning of vacuum systems of new mirror neutron guides on IBR-2 beamlines 13 and 9.

**Detectors and electronics**

In 2017, a new ring gas detector for small-angle thermal neutron scattering was assembled and tested with a neutron source on the RTD diffractometer (IBR-2 beamline 6a). The detector is designed for studies of biological (organic) and nanodispersed polymer objects containing functionally significant inhomogeneities of various structural complexity. A distinguishing feature of the detector is the simultaneous determination of angular and radial coordinates of detected neutrons. A photo of the detector on the test stand is shown in **Fig. II-2-7.**

***Fig. II-2-7.*** *Photo of the detector on the test stand.*

The detector is divided into 9 independent equidistant coaxial rings. The cathodes of each ring are divided into 16 independent sectors forming 144 independent detector elements. The signal pickup is performed from anode wires (shared by all rings) and from each of 16 cathodes. To eliminate the effect of impulse noise and reduce the electronic noise, the preamplifiers of detector elements are arranged inside the gas volume.

Analog electronics for 144 cathode and 9 anode measuring channels have been designed, manufactured and adjusted. Digital electronics for data acquisition and accumulation are based on unified MPD modules and include 5 modules of 32-channel discriminators and an MPD32 controller. Amplitude spectra from all detector rings were obtained (**Fig. II-2-8**). The commissioning on the RTD spectrometer is scheduled for early 2018.

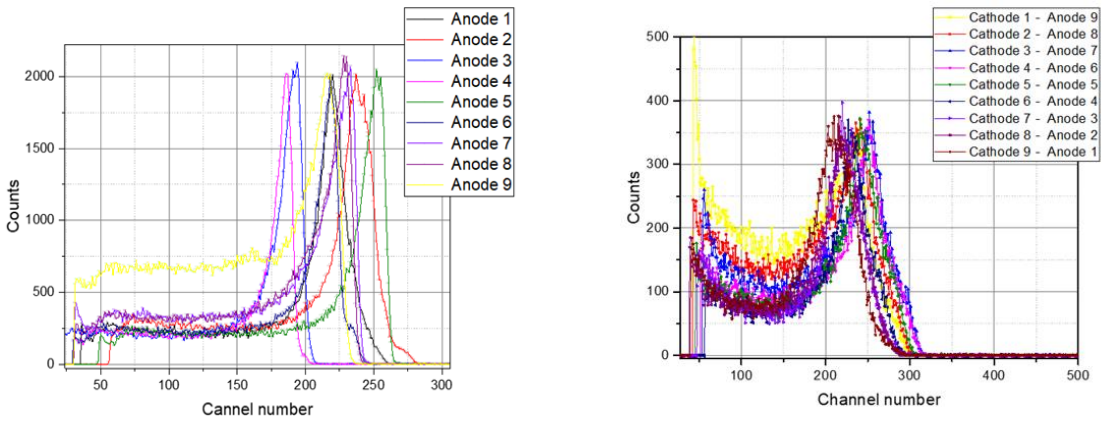


***Fig. II-2-8.*** *Amplitude spectra of a small-angle detector: from anodes (left) and from cathodes (right).*

In 2017, measurements of plasma temperature in the reaction D(d,n)$^3$He were continued using the spectrometer based on a recoil proton telescope, which had been developed in FLNP. Measurements are performed at the National Fusion Research Institute (Daejeon, Republic of Korea) in accordance with the Protocol on Cooperation. Measurements of the background radiation were made and fast neutron spectra were measured at the KSTAR (Korean Superconducting Tokamak Advanced Research) tokamak-type nuclear fusion reactor. Photos of the telescope at the KSTAR facility are shown in **Fig. II-2-9**.

***Fig. II-2-9.*** *Spectrometer on the basis of a proton recoil telescope at the KSTAR nuclear fusion reactor.*

In the framework of the collaborative work on the ESS project (Lund, Sweden), a prototype of PSD on the basis of a multiwire proportional chamber with a $^{10}$B converter has been developed and tested IBR-2 beamline 13 (**Fig. II-2-10**). The coordinate resolution of the detector along the coordinate perpendicular to the anode was measured to be 0.9 mm. The ultimate goal of the work is the development of a 2D neutron PSD with a $^{10}$B converter.

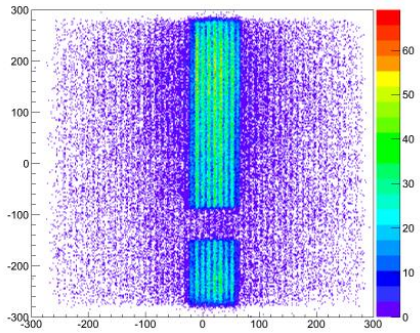

***Fig. II-2-10.*** *Coordinate spectrum obtained on IBR-2 beamline 13.*

In accordance with the technical project for the ASTRA-M detector system (modernized version of ASTRA detector) developed earlier, we continued work on the manufacturing of its main components. The installation of the system on the FSD spectrometer and first test measurements are scheduled for 2018.

The HRFD diffractometer at the IBR-2 reactor is one of three or four neutron diffraction facilities in the world which allows performing experiments at $\Delta d/d \approx 0.001$ or better. At present, the HRFD detector system comprises three detectors, two of which are placed at the scattering angles of ±152°, and the third one at 90°. The detecting elements are Li-glass scintillators. The available HRFD detectors have two disadvantages: small solid angle (~0.16 sr) and high sensitivity to gamma-ray background radiation, resulting in a relatively low data acquisition rate at a sufficiently high neutron flux at the sample position (up to $10^7$ n/cm$^2$/s), and a high background level in the resulting diffraction spectra.

To overcome these drawbacks, the physicists submitted a request to develop a new backscattering detector with an aperture covering the scattering angles 2θ = (133-175)°. For the estimated maximum (80%) of the useful detector area (technological losses may amount to up to ~ 20%) the solid angle is expected to be $\Omega \approx 1.5$ sr, which is almost an order of magnitude higher. To ensure high and ultra-high resolution, the neutron converter will be produced on the basis of a thin (~ 0.4 mm thick) ZnS(Ag)/$^6$LiF scintillator screen, wavelength-shifting fibers and photomultipliers. The production of this type of detectors has been well mastered with the detector system for the FSD spectrometer. In 2017, the detector design was developed and approved, and corresponding contracts were signed for the purchase of necessary materials (primarily scintillators and fiber optics). A schematic of the new backscattering detector is shown in **Fig. II-2-11.**

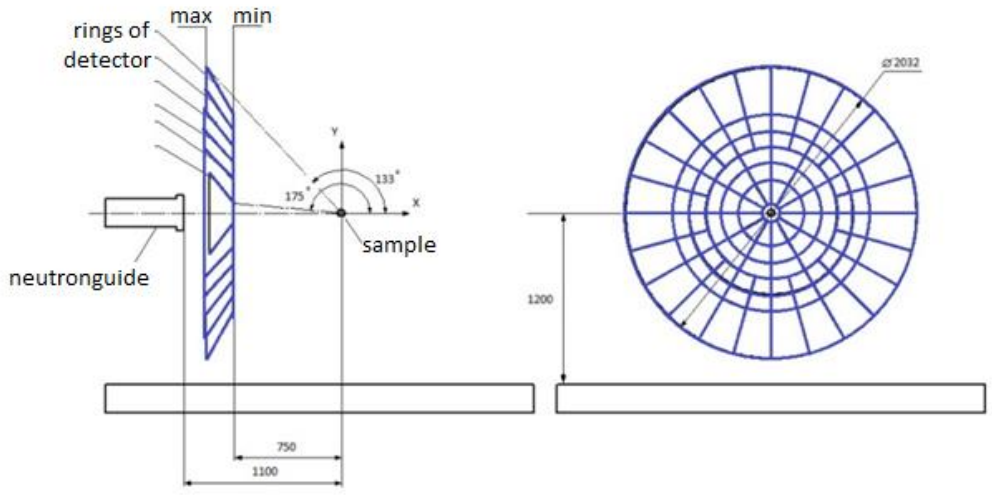


***Fig. II-2-11.*** *Schematic of the backscattering detector with a large aperture (the detector comprises 8 rings, 166 sectors, the solid angle of the detector is ΩD = 1.5-1.8 sr, the total area of the scintillator screen is 13.5 m$^2$).*

All the detectors described above are equipped with the unified blocks of analog and digital electronics and software developed in FLNP. The digital data acquisition systems consist of two basic electronic modules, (De-Li-DAQ11,2 and MPD), one of which processes and accumulates data from one- and two-dimensional PSD, and another – from an array of point detectors (gas and

scintillation counters). All parameters of the modules are programmed. New systems allow one to work both in the histogram mode and in the mode of accumulation of raw data – ListMode (with subsequent off-line processing).

In 2017, work continued on the development of electronics for detector systems. Test programs for accumulating data using multichannel digitizers were written, and 2D coordinate spectra from a neutron source were obtained. For the FSD diffractometer, an MPD accumulation system supplemented with a digital filtering module to select signals from scintillation detectors was developed and implemented.

***Fig. II-2-12.*** *Mobile gas-filling unit.*

At the requests of the researchers, measurements of neutron beam profiles on beamlines 10 and 13 of the IBR-2 reactor were performed using a monitor PSD.

In the framework of the development of the infrastructure of the Detector group, we prepared a technical design specification and signed a contract for the modernization of the clean room for assembling detectors in order to increase its area and enhance its purity class, which will allow us to work with detectors of larger sizes. The installation of climate equipment is scheduled for 2018.

A new mobile gas-filling unit designed to fill detectors with a gas mixture was developed. A photo of the unit is shown in **Fig. II-2-12**. The unit has small dimensions and makes it possible to refill detectors directly in the IBR-2 experimental halls.

**Upgrade of control systems, actuators and sample temperature control systems on IBR-2 spectrometers**

During the reporting period a large amount of work has been carried out to upgrade the actuators of the IBR-2 spectrometers, neutron beam choppers, sample temperature control systems, as well as control systems of these devices. Below are a few examples of these devices.

Due to the adopted architecture of control systems for the actuators of spectrometers, the number of devices for an experimental setup can be increased without any problems in the following way:

- new mechanism is assigned the next number (up to 32);
- "2*OSM42" module is installed in 3U frame at a current of the mechanism stepper motor of less than 4.2 A; each installed module increases the number of control channels in the system by 2;
- "OSM88" module is installed in 3U frame at a current of the mechanism stepper motor of less than 8.8 A;
- if the number of control channels exceeds 32, then the control system is duplicated, and the possible number of control channels increases by another 32;
- parameters of new devices are specified in the system software;
- incorporation of one new control channel into the system takes no more than 2 days.

Following this procedure, the control system of the FSS spectrometer was created. It comprises 6 control channels and 5 modules controlling actuators of the instrument devices including:

- Huber goniometer for sample positioning (coordinates x, y, z; rotation around vertical axis);
- device for positioning Fourier chopper stator.

Two Huber goniometer devices were included into the number of actuators for the REMUR spectrometer, which control the horizontal movement (±30 mm) and inclination (±10°) of the sample. At the SKAT and NERA spectrometers, control systems for experimental setups were upgraded. Control systems of current sources (3 sources with USB interface and 4 sources with control from a programmable source of 0-10 V) were put into operation at the REMUR spectrometer.

On some IBR-2 spectrometers, there is a need for the development of small-size choppers (with their possible use in a vacuum) and corresponding control systems. One of the possible options is to use stepper motors for this purpose. We developed an electronic module and programs for controlling the stepper motor for the chopper prototype (**Fig. II-2-13**). The results of tests of the prototype showed a principal possibility of precise control over the rotation speed of a disk with a diameter of 60 cm and a weight of 5-10 kg.

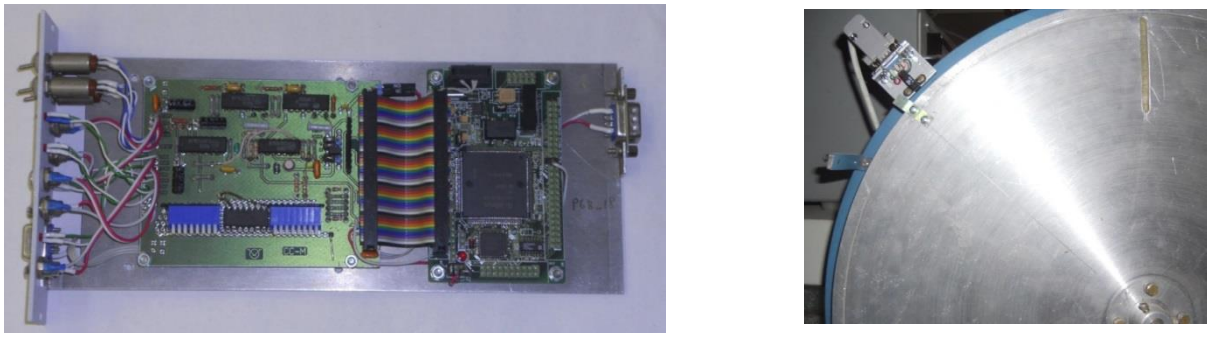

***Fig. II-2-13.*** *Control unit of a stepper motor-driven chopper (left) Prototype of a stepper motor-driven chopper. (right).*

In the framework of modernization of temperature control systems, the replacement of Eurotherm temperature controllers with Lake Shore controllers was completed.

Temperature control systems based on closed cycle cold heads, as well as air and vacuum ovens were put into operation on IBR-2 beamlines 5, 6a, 6b.

**Software and computer infrastructure**

The main focus of the development of Sonix+ software package was on further improvement of the complex, its extension with new components, development of data visualization tools and enhancement of reliability. Among the most important activities were the following:

- development of a new version of the script interpreter module that extends the possibility of direct use of mathematical multidimensional data analysis software packages in the script (Numerical Python, etc.);
- supplementation of a basic set of widgets and improvement of GUI programs – Svetofor program for controlling and monitoring control signals and others;
- development of a new version of SpectraViewer in cooperation with the NICM Department. In this version it is intended to include visualization of spectra in Q space, as well as other useful options. **Figure II-2-14** shows an example of the graph used to search for a reflected beam when tuning reflectometers.

# TECHNICAL DEVELOPMENTS

A Sonix+ version for the FSS diffractometer has been prepared for practical testing and its trial operation has started.

An improved version of WebSonix 4.8 (**Fig. II-2-15**) for remote control over experiments, was developed and put into operation. We added an online spectrum visualization page as well as e-mail notification on the termination of the experiment. At present, eight spectrometers (YuMO, HRFD, FSD, SKAT, NERA, EPSILON, DIN-2PI, REFLEX) have been connected to this service.

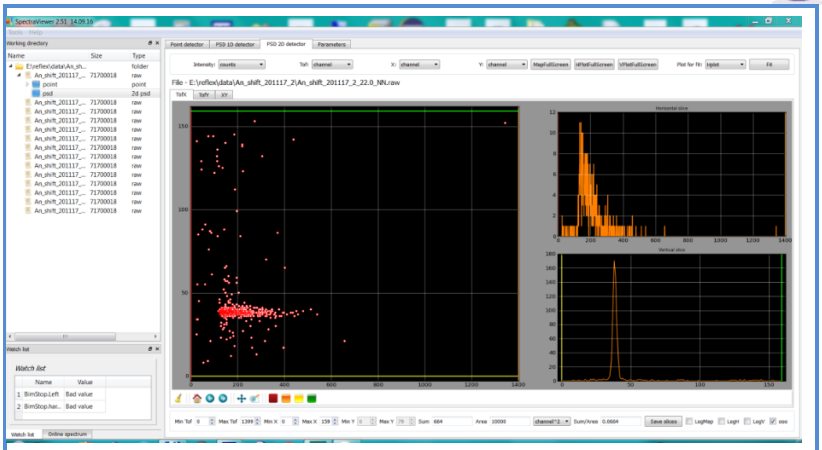

***Fig. II-2-14.*** *New mode of SpectraViewer program to facilitate visual search of the reflected beam when tuning reflectometers.*

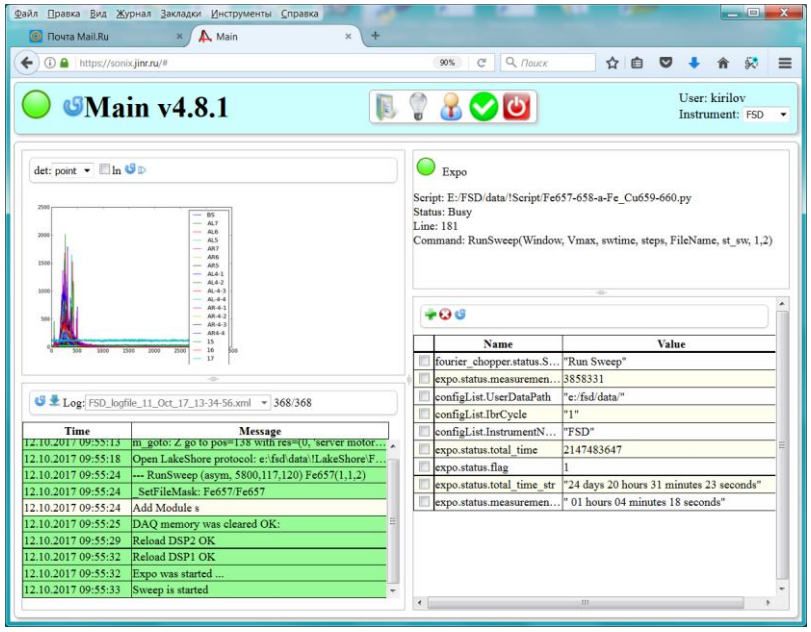


***Fig. II-2-15.*** *Home page of WebSonix service using the example of FSD spectrometer.*

The adaptation and debugging of the Journal program on the GRAINS and HRFD spectrometers are in progress. The program is designed to automatically record measurement results and search for data by individual parameters (user name, measurement time, etc.).

Programs for monitoring the state of the CM-201 cold moderator and a new graphical interface were developed. The development of software tools for debugging and testing digital electronics for data acquisition systems was continued.

The outdated network switches in buildings 42 and 42a were upgraded to provide a data rate of 1 Gbit/s for all end users in the offices of physicists and Directorate of the Laboratory. In the FLNP local area network the number of WiFi access points in buildings 42 and 117 was increased. Six worn-out and outdated network printers were replaced with new models (HP LaserJet M607 dp).